Journal of Drug Delivery Science and Technology 89 (2023) 104963

Contents lists available at ScienceDirect

Journal of Drug Delivery Science and Technology

journal homepage: www.elsevier.com/locate/jddst

A novel high-efficiency transdermal patches for combinational therapy of Alzheimer's disease: Donepezil/vitamin B12-loaded nanofibers

Busra Ertas [a,b], Irem Nur Onay [a], Ayse Mine Yilmaz-Goler [b,c], Betul Karademir-Yilmaz [b,c], Ismail Aslan [d], Muhammet Emin Cam [a,b,e,f,g,h,*]

[a] Department of Pharmacology, Faculty of Pharmacy, Marmara University, Istanbul, 34854, Turkey
[b] Genetic and Metabolic Diseases Research and Investigation Center, Marmara University, İstanbul, Turkey
[c] Department of Biochemistry, Faculty of Medicine, Marmara University, Istanbul, 34854, Turkey
[d] Department of Pharmaceutical Technology, Hamidiye Faculty of Pharmacy, University of Health Sciences, Istanbul, 23668, Turkey
[e] Center for Nanotechnology and Biomaterials Application and Research, Marmara University, Istanbul, 34722, Turkey
[f] Biomedical Engineering Department, University of Aveiro, 3810-193, Aveiro, Portugal
[g] Department of Pharmacology, Faculty of Pharmacy, Istanbul Kent University, Istanbul, 34406, Turkey
[h] MecNano Technologies, Cube Incibation, Teknopark Istanbul, Istanbul, 34906, Turkey

ARTICLE INFO

Keywords:
Alzheimer's disease
Donepezil
Vitamin B12

ABSTRACT

Improving clinical practice in disease-modifying therapies is an important strategy in coping with the progressive course of Alzheimer's Disease (AD). This study aimed to develop DO and VB12-loaded nanofibers (DO/VB12-loaded NFs) as a transdermal drug delivery system, examine physicochemical properties, and evaluate the *in vitro* anti-Alzheimer's activity. DO/VB12-loaded NFs were produced with enhanced properties and a smooth structure without bead formation by the pressured gyration method. The drugs showed rapid release from DO/VB12-loaded NFs on the first day followed by sustained release for 14 days, indicating their suitability for transdermal application. Furthermore, the anti-Alzheimer's potential of DO/VB12-loaded NFs was investigated in a wide range using the functional ability of mitochondria (MTT) and viability analysis in amyloid-β (Aβ)-induced SH-SY5Y cells. The *in vitro* AD activity of DO/VB12-loaded NFs has been demonstrated as they are not cellular cytotoxic, promote viability in SH-SY5Y cells against $A\beta_{1\text{-}42}$-induced neurotoxicity, and decrease gene expressions of APP and BACE-1, increase ADAM-10. In addition, cell morphology was visualized by confocal microscopy after treatment with DO/VB12-loaded NFs. Overall, those data showed that the designed NFs are a promising alternative to deliver DO and VB12 transdermally for the treatment of AD.

1. Introduction

Alzheimer's disease (AD) is an age-related debilitating brain disorder that will impact 150 million people by 2050 [1]. AD has become a significant burden on their families and society due to the inadequacy of therapeutic options [2]. The widespread mechanism underlying AD consists of the amyloid and acetylcholine hypothesis. Abnormal aggregation of amyloid-β (Aβ), amyloid fibrils, and amyloid plaques triggers neurotoxicity, neurite injuries, and proinflammatory response. Current studies focus on investigating options Aβ reducing therapeutic agents [3]. Although acetylcholinesterase inhibitors (ACEIs) provide efficacy in the treatment of moderate-to-severe AD, their monotherapies limit this efficacy, thus necessitating combined therapy [4]. In addition, conditions that may occur as a result of oral administration, such as adverse drug reactions, multiple daily dosing, and drug-drug interactions, predispose to treatment non-adherence, especially in elderly patients [5]. The effects of the aforementioned drawbacks can be mitigated by the use of transdermal patches which can provide long-lasting effects with single-dosing and multi-drug release.

Donepezil (DO), as an ACEI, increases cholinergic activity in the cerebral cortex, which plays an important role in memory and learning, as a result of preventing the breakdown of acetylcholine [6,7]. Increasing evidence showed that DO prevents Aβ-induced neuronal damage with its microglia deactivating effect and shows memory-protecting effects as a receptor-independent effect (non-cholinergic mechanisms) [8]. The low water solubility, poor bioavailability,

* Corresponding author. Department of Pharmacology, Faculty of Pharmacy, Marmara University, Istanbul, 34854, Turkey.
E-mail address: muhammet.cam@marmara.edu.tr (M.E. Cam).

https://doi.org/10.1016/j.jddst.2023.104963
Received 2 April 2023; Received in revised form 16 September 2023; Accepted 16 September 2023
Available online 17 September 2023
1773-2247/© 2023 Elsevier B.V. All rights reserved.

Table 1
Polymer contents of the solutions.

Fiber	Polymer ratio (v/v)	PCL content (%, w/v)	PVP content (%, w/v)
10PF41	PCL/PVP (4:1)	10	10
10PF32	PCL/PVP (3:2)	10	10
15PF41	PCL/PVP (4:1)	15	15
15PF32	PCL/PVP (3:2)	15	15
20PF41	PCL/PVP (4:1)	20	20
20PF32	PCL/PVP (3:2)	20	20

Table 2
PCR primer sequences were used.

Gene Symbol	Primer Sequences
APP	Forward 5'-TCAGTCTCTCTCCCTGCTCT-3' Right 5'-GGTGGTTTTCGTTTCGGTCA-3'
BACE-1	Forward 5'-TCCCATTGGTCTGCATGTCT-3' Right 5'-AGCGCCTCAGTGTTACTCTT-3'
ADAM10	Forward 5'-GGGCTGTGCAGATCATTCAG-3' Right 5'- TTCCGGAGAAGTCTGTGGTC-3'
GAPDH	Forward 5'-CCAAGGAGTAAGACCCCTGG-3' Right 5'-AGGGGAGATTCAGTGTGGTG-3'

and short half-life of DO, as well as the gastrointestinal side effects such as diarrhea, nausea, and vomiting due to sudden changes in plasma concentration, are important clinical limitations [9]. Vitamin B12 (VB12), which is necessary for nervous system functions, is found to be low in patients with AD [10]. VB12 deficiency causes an increase in radical oxygen species (ROS), resulting in decreased brain-derived neurotrophic factor (BDNF) and neural growth factor (NGF) levels and neuronal damage [11]. According to the results of clinical studies, the therapy of VB12 for 6 months improved cognitive performance and decreased the level of inflammatory cytokines in the blood [12]. Lam et al. showed that VB12 protects from Aβ-induced proteotoxicity by a mechanism dependent on the methionine/S-adenosylmethionine (SAMe) cycle [13]. Andrade et al. [14] has shown that VB12 reduces amyloid fibrillation in the existing artificial neuronal membrane. In addition, VB12 inhibits Aβ formation by reducing BACE1 expression in the SH-SY5Y neuroblastoma cell line [15]. While these results support the pharmacological potential of VB12, its low and highly variable oral absorption due to its hydrophilic nature reduces the therapeutic efficacy [16]. Aβ occurs by proteolytic degradation of APP and is one of the clinical biomarkers of AD. α-secretase (ADAM10) activity inhibits APP formation, while β–secretase (BACE-1) activity is the rate-limiting step in Aβ peptide production from APP. Since the altered activity of these proteins in the brain correlates with amyloid formation, it is considered a therapeutic target [17].

A transdermal patch for drug delivery is notable not only for its non-invasiveness but also thanks to exhibiting relatively few side effects compared to conventional therapy [18]. From this perspective, transdermal drug delivery systems are a conceivable option to overcome the difficulties experienced in oral drug use in Alzheimer's patients [19]. In this study, we designed DO/VB12-loaded nanofibers (NFs) that remove the bioavailability limitation of DO and VB12, which are effective in AD-related pathologies and offer combination therapy, targeting effective treatment with a prolonged release. DO is a small molecular weight of 379.5 g/mol (free base) and is lipophilic (log p-value of 3.08–4.11) (PubChem CID: 9651). With such physicochemical properties and therapeutic profile, it is considered a well-suited candidate for transdermal delivery [18]. The bioavailability of VB12 is generally assumed to be 40 or 50% for adults [20]. Its high molecular weight, which prevents it from crossing the blood-brain barrier, and its hydrophilic structure, which reduces its absorption, limit clinical practice [21]. Hydrophilic drugs can be effectively delivered through the skin with the high surface area/volume ratio of the fibers. In transdermal systems, it is necessary to overcome the permeability barrier in the skin (stratum corneum) for drug delivery [22]. Therefore, we aimed to provide improved bioavailability with the physicochemical properties of the polymer-based NFs. Polycaprolactone (PCL) can help the penetration of water-soluble drugs such as VB12 and DO from the lipophilic skin with its hydrophobic nature. Polyvinyl pyrrolidone (PVP) is a biodegradable, non-toxic, and hydrophilic synthetic polymer. Moreover, it is compatible with other polymers and suitable to blend with PCL as it can interact with both hydrophilic and hydrophobic materials [23].

This background allowed us to hypothesize that the efficacy of DO and VB12 combination in the treatment of AD can overcome the bioavailability problem of drugs with the transdermal patch formulation by pressurized gyration. Thus, in the present study, we specifically focused on preparing, enhancing, and evaluating a new nanofibrous formulation and nano-delivery system of PCL/PVP loaded with DO and VB12 for therapeutic purposes AD. Furthermore, AD-related biological activities of DO/VB12-loaded NFs were evaluated in detail by *in vitro* tests, including cytotoxicity testing, neuroprotective effect in $A\beta_{1\text{-}42}$-induced cells, and effect on the expression of genes involved in amyloid formation.

2. Materials and methods

2.1. Materials

Donepezil (DO, Mw ~ 379.492 g/mol), Vitamin B12 (VB12, Mw ~ 1355.37 g/mol), Polycaprolactone (PCL, Mw ~ 80,000 Da), Polyvinyl pyrrolidone (PVP, Mw ~ 40,000 Da), chloroform (99.9%, v/v), methanol (99.9%, v/v), and ethanol (99.9%, v/v) were purchased from Sigma Aldrich. All chemicals were analytical grade, and all biological agents were cell culture grade and used without further sterilization.

2.2. Preparation of solutions and fabrication of fibers

The solutions of PCL and PVP (10, 15, and 20% (w/v)) were dissolved in chloroform:methanol (3:1, v/v) solvent [24]. PCL and PVP solutions prepared at different w/v ratios were mixed at specified (3:2 and 4:1, v/v) ratios, respectively (Table 1). The resulting solutions were prepared separately and stirred with a magnetic stirrer for at least 24 h at room temperature to ensure a homogeneity [25]. The morphology and size of six pure fibers (PF) were investigated and the best solution was chosen as 15PF41 which has better fiber formation according to scanning electron microscopy. Then, 5 mg/ml DO and 5 mg/ml B12 were added to the optimum ratio (15PF41) of PCL/PVP [26,27]. DO/VB12-loaded NFs were fabricated by the pressurized gyration method. The pressurized gyration method uses centrifugal spinning force and gas pressure to produce fibers. 1 ml of mixture solutions was placed in a stainless steel pot sized 41 mm × 60 mm with multiple 1.0 mm diameter rounded holes. Fiber productions were performed under various conditions (20–40 °C, 30–60% humidity) with 6000–12,000 rpm rotational speed and 0.1–0.4 MPa working pressure [28].

2.3. Scanning electron microscopy (SEM)

The diameter and morphology of the fibers manufactured by the pressurized gyration technique were observed and determined after high-resolution images were captured by scanning electron microscopy (SEM device; EVO LS 10, Zeiss, Germany). The surface of the samples was electrically conductive by coating them with a thin layer of gold for 60 s. The working distance was 25 mm and the accelerating voltage was 5 kV. The average fiber diameter and size distribution were specified by analyzing 100 fibers and all the data were analyzed via image software ImageJ (Brocken Symmetry Software) to assess the mean diameter [25].

2.4. Fourier transform infrared spectroscopy (FTIR)

FTIR measurements were performed to analyze the molecular

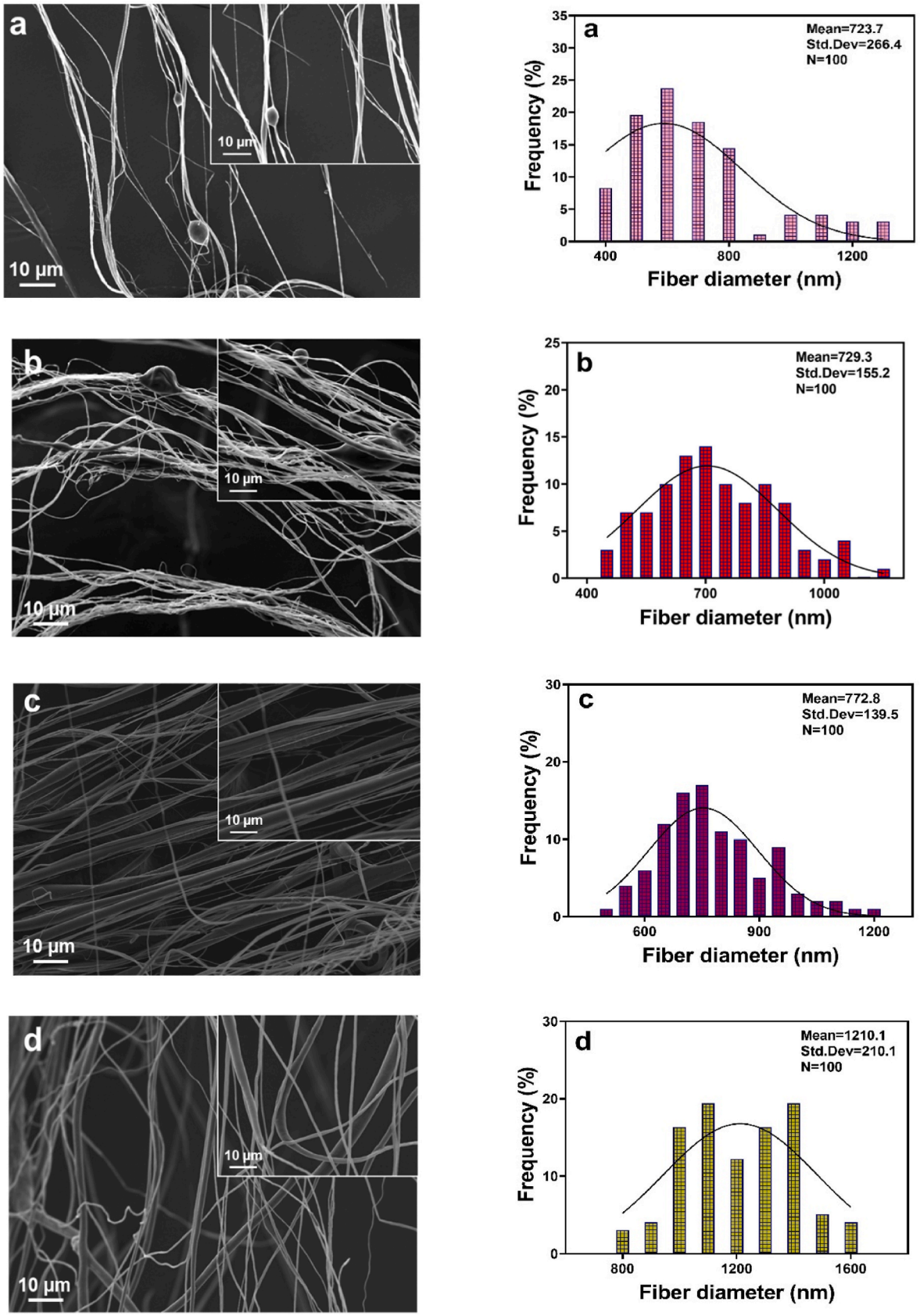

Fig. 1. SEM images and fiber diameter distribution of pure polycaprolactone (PCL)/pure polyvinyl pyrrolidone (PVP) fibers at six different ratios: (a) 10PF41, (b) 10PF32, (c) 15PF41, (d) 15PF32, (e) 20PF41, (f) 20PF32, and also (g) DO/VB12-loaded NF.

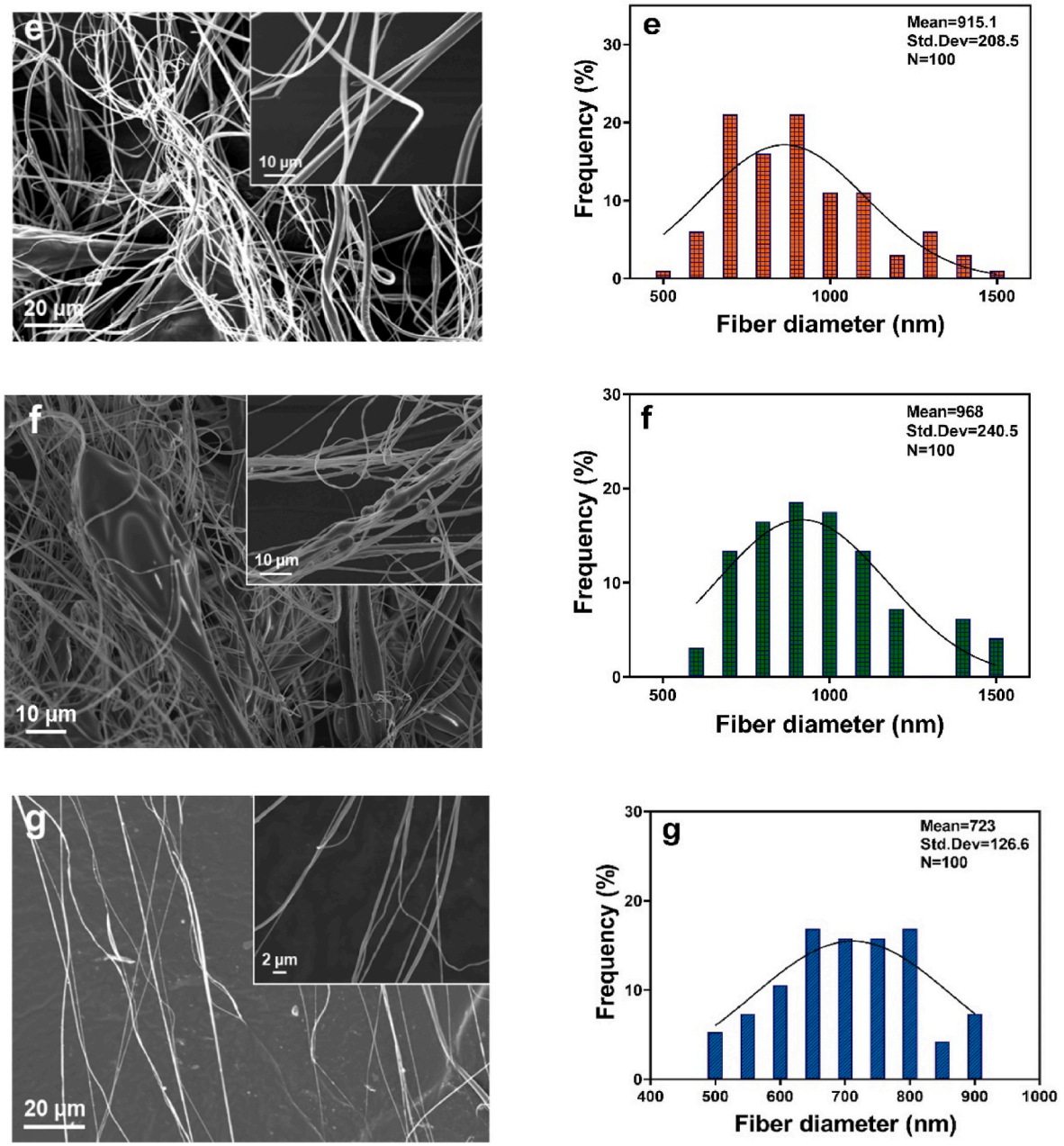

Fig. 1. (*continued*).

contents of DO/VB12-loaded NFs and PF. FTIR spectroscopy was realized using a Spectrum 100 FTIR spectrometer fitted with an ATR attachment. Measurements were carried out using a Jasco FTIR 4700 spectrometer in the wavelength region 400 and 4000 cm^{-1} in transmission mode with a resolution of 4 cm^{-1}. Spectrographs were collected at room temperature and studied with OPUS Viewer version 6.5 software [29].

2.5. X-ray powder diffraction (XRD)

Structure and crystalline forms of fiber contents were recorded using XRD–diffractometer (RigaKu, Tokyo, Japan) with Cu Kα radiation. The XRD patterns were examined at 40 mV and 30 mA over a 2θ range of 0–80° at a rate of 2°/min. OriginPro 7.0 software (OriginLab Corporation, MA, USA) was used to convert the obtained data to diffractograms and for their evaluation.

2.6. Thermal properties of fibers

The thermal behaviour of the fibers was determined using differential scanning calorimetry (DSC) (Shimadzu, Japan). The system was set at a temperature ranging from 0 to 350 °C under a dynamic argon atmosphere (20 ml/min) with a controlled heating rate of 10 °C min^{-1}. Approximately 10 mg of each sample was placed in the aluminum pan and folded. The melting temperature (Tm), glass transition temperature (Tg), and crystallization temperature (Tc) of composite fibers were established from the DSC curves [30].

2.7. Drug encapsulation efficiency

Drug encapsulation efficiency is a quantitative determination of the drug content of fibers and is described as the weight ratio of the actual to the theoretical amount of drug loaded into fibers. 5 mg of DO/VB12-loaded NFs dissolved in 10 ml of their solvent mixtures in a

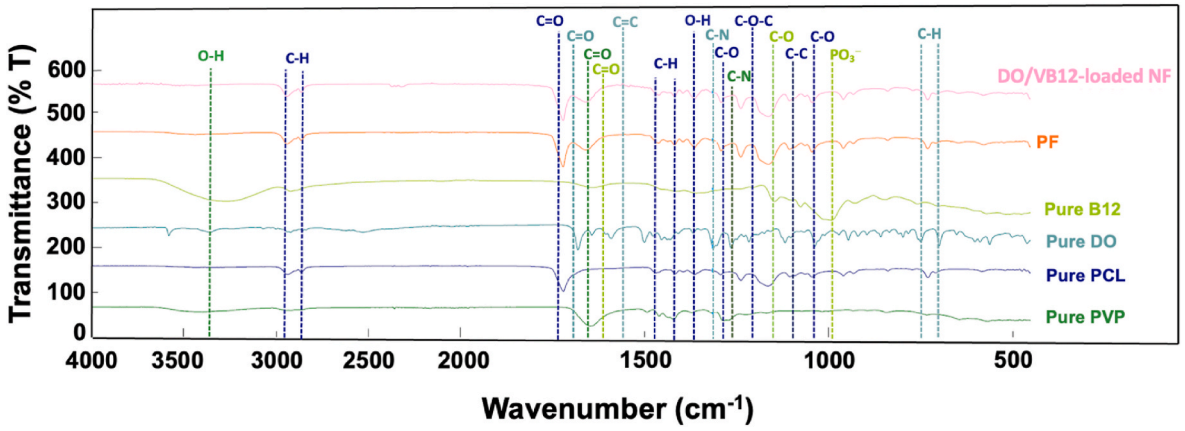

Fig. 2. Fourier-transform infrared spectroscopy (FTIR) spectrums of pure polycaprolactone (PCL), pure polyvinyl pyrrolidine (PVP), donepezil (DO), Vitamin B12 (VB12), pure PCL/PVP nanofiber (PF), and DO/VB12-loaded NF produced by pressurized gyration.

volumetric flask and mixed slowly with a magnetic stirrer for 1 h to provide complete dissolution. 1 ml of solution was evaluated using UV spectroscopy (Shimadzu UV-3600, Japan) at 271 nm for DO and 365 nm for VB12 [22,31]. The % encapsulation efficiency was calculated using the equation given below [32]. All measurements were analyzed in triplicate each time.

$$Encapsulation\ efficiency = \frac{mass\ of\ actual\ drug\ loaded\ in\ fibers}{mass\ of\ drug\ used\ in\ fibers\ fabrication} x100\% \quad (1)$$

2.8. In vitro drug release test

The release profile of DO and VB12 from DO/VB12-loaded NFs was studied in phosphate-buffered saline (PBS) at pH 7.4. Each DO/VB12-loaded NF sample (5 mg) was incubated at 37 °C in 10 ml of the PBS release medium under shaking [22]. Samples (1 ml) were taken from the release medium at certain periods (0, 15, 30, 45, 60, 90, 120, 180, 240, 360, 480, 720 min, and then every day for 14 days) and that volume was replaced with fresh PBS. DO and B12 were analyzed using a linear calibration curve in the 5 different concentrations (2, 4, 6, 8, and 10 μg/ml). 1 ml of solution was evaluated using UV spectroscopy (Shimadzu UV-3600, Japan) at 271 nm for DO and 365 nm for B12 [22,31].

2.9. In vitro drug release kinetics

DO and VB12 release kinetics were investigated by model-dependent methods based on five different mathematical functions. The model-dependent mathematical functions known that zero order (Eq (2)), first order (Eq (3)), Higuchi (Eq (4)), Hixson-Crowell (Eq (5)), and Korsmeyer-Peppas (Eq (6)) were represented below [33].

$$Q = K_0 t \quad (2)$$

$$\ln(1 - Q) = -K_1 t \quad (3)$$

$$Q = K_h t^{1/2} \quad (4)$$

$$Q^{1/3} = K_{hc} t \quad (5)$$

$$Q = Kt^n \quad (6)$$

Zero order, first order, Higuchi, Hixson-Crowell, and Korsmeyer-Peppas models were represented by K, K_0, K_1, K_h, and K_{hc}, which are the kinetic constants, respectively. In addition, Q is the fractional amount of drug release at time t. n is the diffusion exponent, which is indicative of the drug release mechanism.

2.10. Franz cell diffusion test

The Franz diffusion method was used to investigate the transdermal permeation of drugs from DO/VB12-loaded NFs *in vitro*. The receptor chamber of the Franz diffusion cell containing 10 ml of PBS (pH 7.4) with a stir bar was placed on the magnetic stirrer. The donor chamber was empty and open to the air, representing the skin surface [34]. The cellulose acetate membrane with a pore size of 0.45 μm was mounted horizontally between the donor and the receptor chambers. DO/VB12-loaded NFs were placed onto the membrane and two chambers were compressed by clamps. On the other hand, DO and VB12 solutions were prepared and put into the donor chambers separately to compare these drugs' release from the NFs. Thus, the effect of NFs on prolonged drug release can be observed. The receptor chamber was kept at a constant temperature of 37 °C throughout the test. 1 ml solution was taken from the sampling port then 1 ml of PBS was added at certain times (0.5, 1, 2, 3, 4, 16, and 24 h) and the solution was evaluated using UV spectroscopy (Shimadzu UV-3600, Japan) [35].

2.11. Degradation assay

Swelling rates of DO/VB12-loaded NFs were evaluated by allowing fibers to swell in PBS (pH 7.4 at 37 °C) solution. All fibers placed in 1 ml of PBS were kept on a 37 °C thermal shaker (BIOSAN TS-100) throughout the experiment. The initial weights (W_o) of fibers were measured on the first day. Then, after swelling, the wet weights (W_w) of fibers are weighed at defined times (at 2, 4, 6, 8, 10, 12, and 24th h) in a day. The swelling value (S) was calculated according to Eq (7) [32].

$$S = (Ww - Wo) \ / \ Wo\ x\ 100 \quad (7)$$

Fibers saturated in PBS solution were dried at ambient conditions for 6 h and their weights (W_t) were measured every 3 days (1, 4, 7, 10, 13, 16, 19, 22, 25, 28, 31, 34, 37, and 40th). The level of degradation (D_i) was calculated according to Eq (8) [32].

$$Di = (Wo - Wt) \ / \ Wo\ x\ 100 \quad (8)$$

2.12. Cell cultures

The human neuroblastoma cells SH-SY5Y (ATCC; CRL-2266) Dulbecco's modified Eagle's medium/F12 mixture medium (1:1) under appropriate conditions (humidified 5% (v/v) CO_2/air at 37 °C) 10% (v/v) were cultured in fetal bovine serum (FBS) and 1% penicillin/streptomycin. Cells were seeded in flasks and the differentiation process of cells was followed by light microscopy for 10 days. Passaged when it reaches 70–80% confluence.

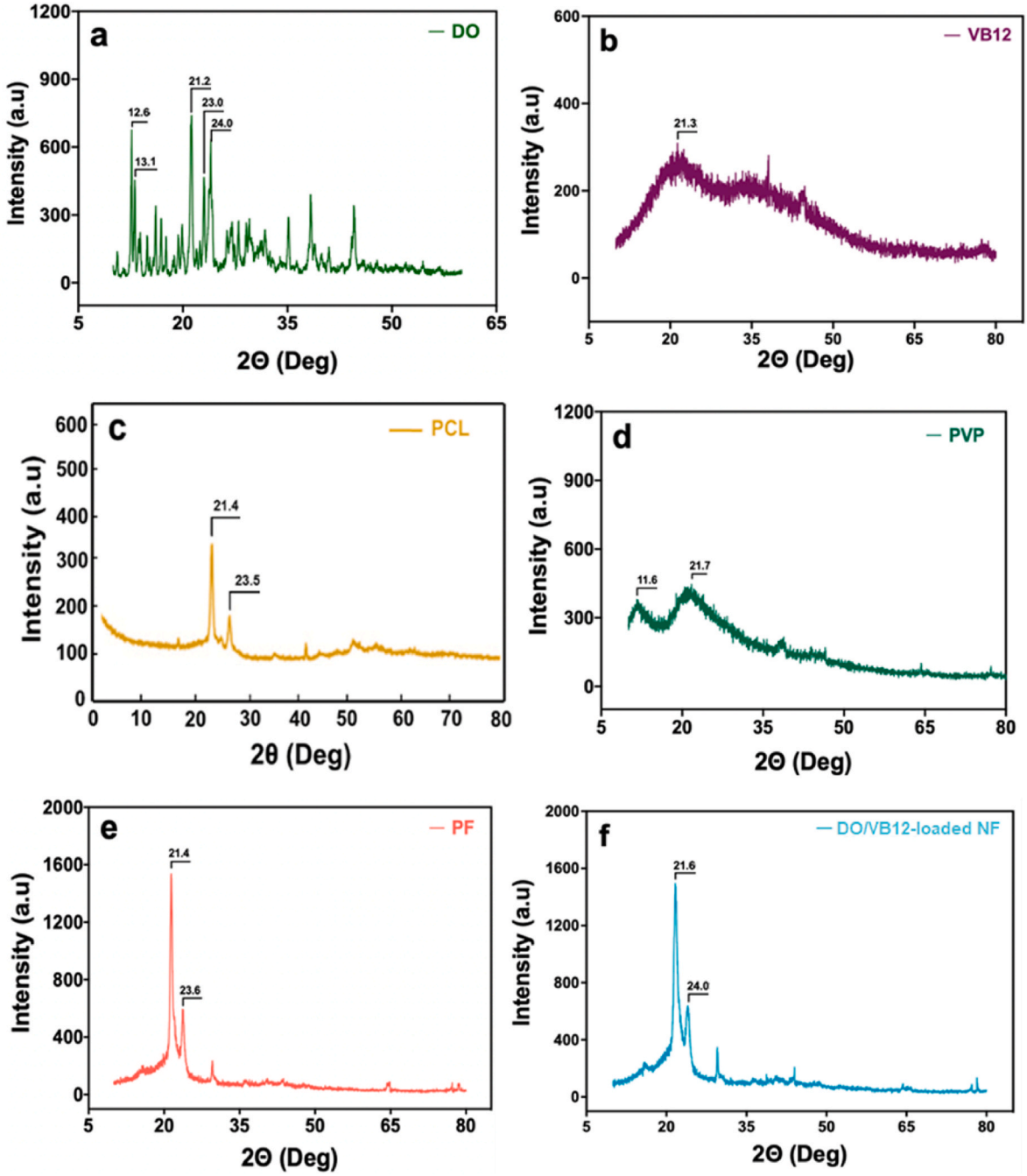

Fig. 3. X-Ray powder diffraction (XRD) results of (a) donepezil (DO), (b) vitamin B12 (B12), (c) polycaprolactone (PCL), (d) polyvinyl pyrrolidone (PVP), (e) pure PCL/PVP nanofiber (PF), and (f) DO/VB12-loaded NF produced by pressurized gyration.

2.12.1. The cellular model of AD and treatments

Peptides were prepared as in previous studies. Briefly, 1 mg of Amyloid-β_{1-42} ($A\beta_{1-42}$; Sigma-Aldrich, St. Louis MO, USA) was dissolved in anhydrous DMSO and incubated at 37 °C for 4 days [36]. The prepared solution of amyloid peptide diluted in the medium was passed through a 0.22 μM filter and applied to cells. Simultaneously with this preparation, the monitoring of the cells continued.

2.13. The cellular model of AD and treatments

The SH-SY5Y cells were treated as follows:

(1) Control group: Incubated in a medium (as appropriate) solution for 24 h;
(2) $A\beta_{1-42}$ group: Incubated in a medium solution containing $A\beta_{1-42}$ (5 μM) for 24 h;
(3) $A\beta_{1-42}$ + pure NF treatment: Incubated in a medium solution containing $A\beta_{1-42}$ (5 μM) for 24 h and then post-incubated with pure NFs (50-100-200 μM) for 12 h;
(4) $A\beta_{1-42}$ + DO/VB12-loaded NF treatment: Incubated in a medium solution containing $A\beta_{1-42}$ (5 μM) for 24 h and then post-incubated with DO/VB12-loaded NFs (50-100-200 μM) for 12 h.

2.14. MTT assay

The cytotoxicity and cell viability (presence with amyloid-β_{1-42}) of pure and DO/VB12-loaded NFs in SH-SY5Y cells treated were evaluated using the MTT (3-(4,5-dimethyl- thiazol-2-yl)-2,5-diphenyltetrazolium

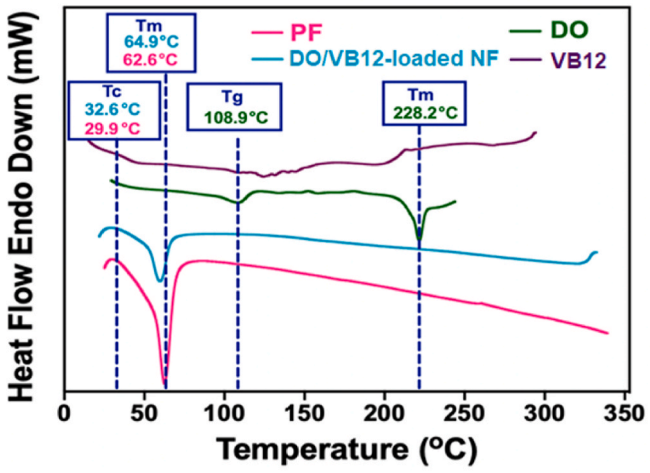

Fig. 4. DSC result of donepezil (DO), vitamin B12 (VB12), polycaprolactone (PCL), polyvinyl pyrrolidone (PVP), pure PCL/PVP fiber (PF), and DO/VB12-loaded NF produced by pressurized gyration.

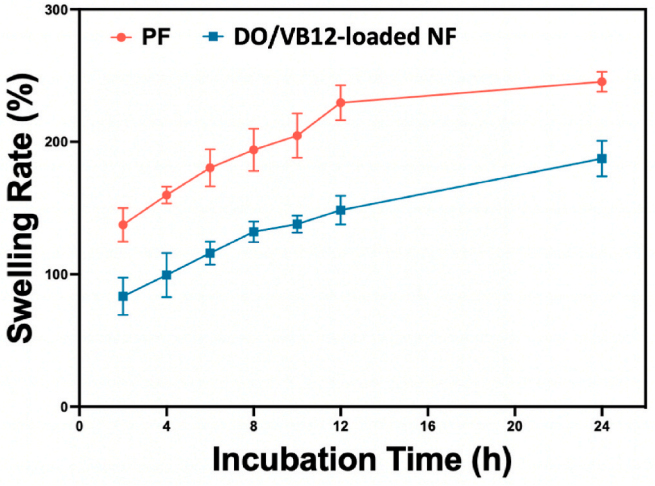

Fig. 5. Swelling rates of pure PCL/PVP nanofiber (PF) and DO/VB12-loaded NF.

bromide) assay. MTT generated reduction with active mitochondrial reductase to form purple formazan crystals in living cells [37]. SH-SY5Y cells seeded in a 96-well plate (5000 cells/well) were treated with various doses of pure and DO/VB12-loaded NFs. Cells were incubated with 0.5 mg/ml MTT for 4 h at 37 °C following treatment. DMSO was added to the medium to dissolve the formed formazan crystals. After 20 min, absorbance was measured (Perkin Elmer, Boston, USA) at 570 nm. To evaluate the anti-Alzheimer's efficacy *in vitro*, the effect of DO/VB12-loaded NFs on the viability of cells in the presence of $A\beta_{1-42}$ (5 μM) was determined by the MTT assay (procedure followed the previous stage). This method was applied by modifying the study of Alam et al. [37]. The confluent cells were observed with SEM investigations in cytotoxicity tests at the most effective concentration of PF and DO/VB12-loaded NF treatments. The cell viability tests (n = 5) were performed in triplicate. The average of the results obtained was presented.

2.15. Real-time polymerase chain reaction (RT-PCR)

SH-SY5Y cells (2.5×10^5 cells/well) were seeded in a 6-well plate. After being treated with 5 μM $A\beta_{1-42}$ for 12 h, DO/VB12 free drug combination and DO/VB12-loaded NF were treated for 6 h. Total RNA was isolated from the cells using the MiniRNeasy Kit (Qiagen, Hilden, Germany) and cDNA was synthesized using the Qiagen First Strand Kit, and quantified using a Biotech Spectrophotometer. RT^2-PCR was performed using the RT^2-PCR SYBR Green FAST Mastermixes (Qiagen, CA, USA) on the Rotor-Gene Q System (Qiagen, Hilden, Germany). The primer sequences that were used are presented in Table 2. The primers used in the present study were obtained from the Primer Bank. In the analysis, relative results were calculated using the $2^{-\Delta\Delta Ct}$ method to normalize cycle threshold (Ct) values according to reference genes using PCR Array Data Analysis Software (The GeneGlobe Data Analysis Center, Qiagen). Ct values allowed us to analyze fold changes in gene expression. Data were considered as the GAPDH gene control.

2.16. Confocal microscopy

SH-SY5Y cells were seeded onto 24-well glass-bottom confocal plates at a cell density of 1×10^5 in the medium. Then incubated for 36 h, the medium was replaced with fresh medium containing $A\beta_{1-42}$ 5 μM. After 24 h, DO/VB12-loaded NF therapy was administered. After 12 h of treatment, cells were washed 3 times with PBS and fixed with fresh 4% paraformaldehyde for 10 min. The membrane was washed with 0.1% Triton X-100 for permeabilization. Subsequently, cells were incubated with Alexa 488 (Santa-Cruz Biotechnology) for 1 h. After washing 3 times with PBS, for visualization, cell nuclei were stained with DAPI (49,6-diamidino-2-phenylindole). Dyes were added in the dark and contact with light was avoided during incubation. Finally, cells were visualized with a confocal scanning microscope (Zeiss LSM700). The excitation and emission wavelengths are 488 nm and 500 nm for Alexa 488; 364 nm and 460 nm for DAPI, respectively.

2.17. Statistical analysis

Data analysis was performed using GraphPad Prism 9.0 software (Graph Pad, San Diego, CA, USA). Analysis results are presented as mean ± standard error of the mean except for fiber distribution graphs, which are presented as mean ± standard deviation, and the interactions between different groups were tested using one-way analysis of variance (ANOVA), Tukey's honest difference was conducted as post-doc analysis. The values of $p < 0.05$ were considered significant.

3. Results

3.1. Morphological characterization of fibers

In this study, the optimum ambient conditions for the production of fibers were determined as 56% humidity and 25 °C temperature. The production of 15PF41 and DO/VB12-loaded NF was optimized under various conditions with 12,000 rpm rotational speed and 0.15 MPa working pressure.

The morphology of PF at six different polymer concentrations produced by pressurized gyration was analyzed using SEM to determine the optimized polymer ratio to use for drug loading. Fiber structures, diameters, and size distributions were compared and the results were given in Fig. 1. The diameters of 10PF41, 10PF32, 15PF41, 15PF32, 20PF41, and 20PF32 fibers were 723.7 ± 266.4, 729.3 ± 155.2, 772.8 ± 139.5, 1210.1 ± 210.1, 915.1 ± 208.5, and 968 ± 240.5 nm, respectively. It was observed that among PCL and PVP solutions with the same w/v concentration, blends with a higher PCL ratio (i.e., 10PF41 vs. 10PF32) had a lower mean fiber diameter. Also, the largest fiber diameter belonged to 15PF32. Although 10PF41 fiber had the smallest diameter, the size distribution was not consistent (Fig. 1a). Beaded and nonhomogeneous fibers were obtained with 10PF41, 10PF32, 20PF41, and 20PF32 (Fig. 1a, b, 1e, and 1f, respectively). The surfaces of 15PF41 and 15PF32 were smooth as seen in SEM images (Fig. 1c and d, respectively). Ultimately, 15PF41 fiber was chosen as the optimized

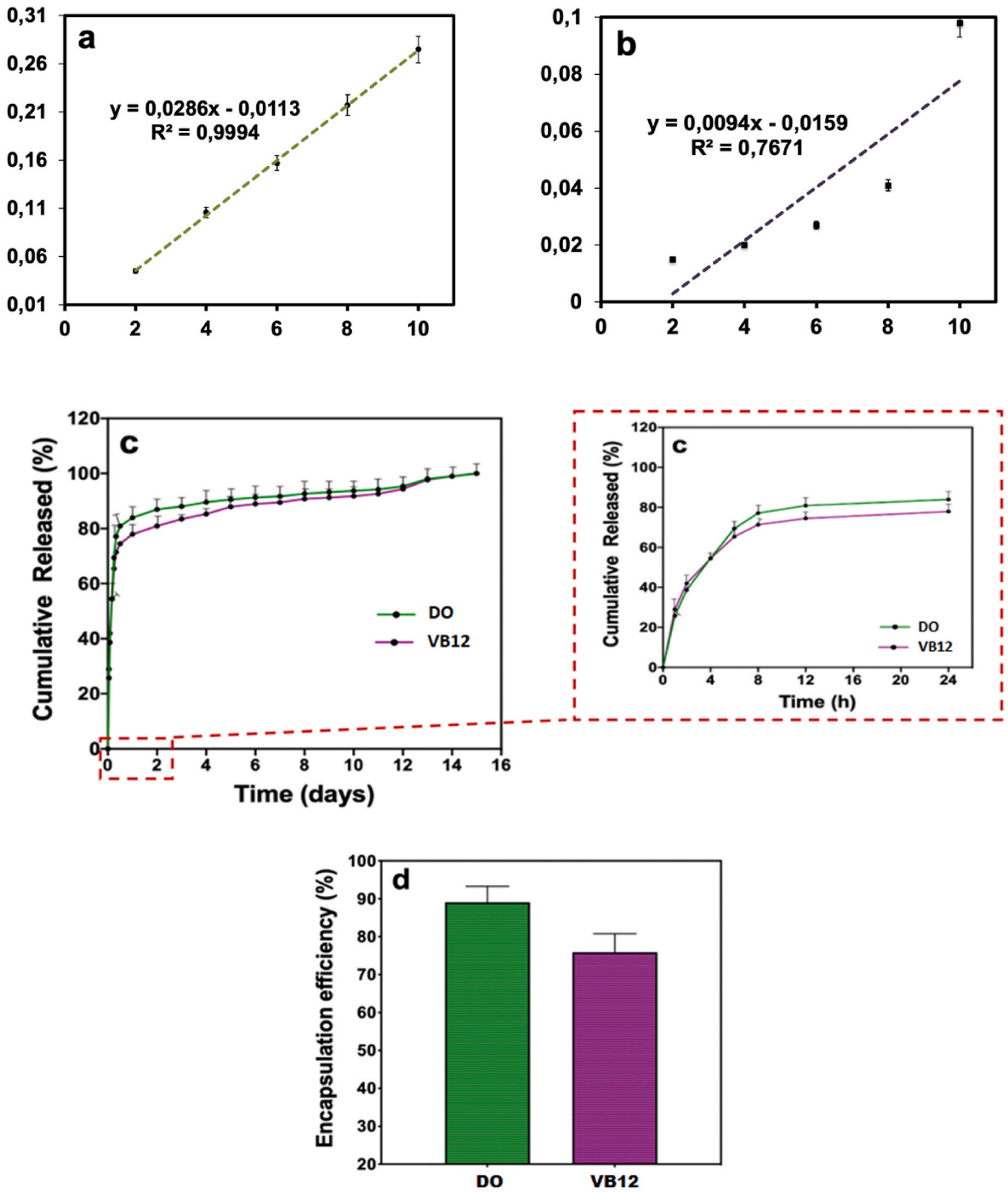

Fig. 6. *In vitro* drug release profiles of NFs: (a) DO calibration curve, (b) VB12 calibration curve, (c) DO and VB12 release profile from DO/VB12-loaded NFs, (d) encapsulation efficiencies of DO/B12-loaded NFs. All the values were obtained from the averages of three measures, and the errors were less than 5%.

composite ratio with its superiority in morphology and more uniform fiber diameter distribution compared to others. After the determination of the optimized ratio of polymers, DO and VB12 were loaded into the same ratio (15PF41) and the changes in the morphology were investigated. As the diameter distribution in Fig. 1g shows, the diameter of the NFs decreased with the addition of DO and VB12.

3.2. Analysis of fiber composition

As an effective method, FTIR characterization is generally used to investigate molecular-specific interactions in polymer mixtures owing to its private sensitivity to the polymer microstructure [38]. Therefore, FTIR spectra were evaluated to show the existence of PCL, PVP, DO, and B12 in DO/B12-loaded NFs and Fig. 2 represents the FTIR spectrum in the wavelength range of 4000–400 cm^{-1} are shown. The FTIR spectra of pure PCL, two bands at 2944 and 2867 cm^{-1} correspond to the C–H asymmetric and symmetric stretching in methylene (CH_2) groups, respectively [26]. Besides, the characteristic stretching vibration of C═O belongs to the ester carbonyl group at 1721 cm^{-1}. In addition, the peaks located at 1470 and 1417 cm^{-1} mainly correspond to C–H bending, and the peaks located at 1396 and 1364 $cm^{-1}$are match O–H bending. Moreover, the peaks located at 1239 and 1162 cm^{-1} comply

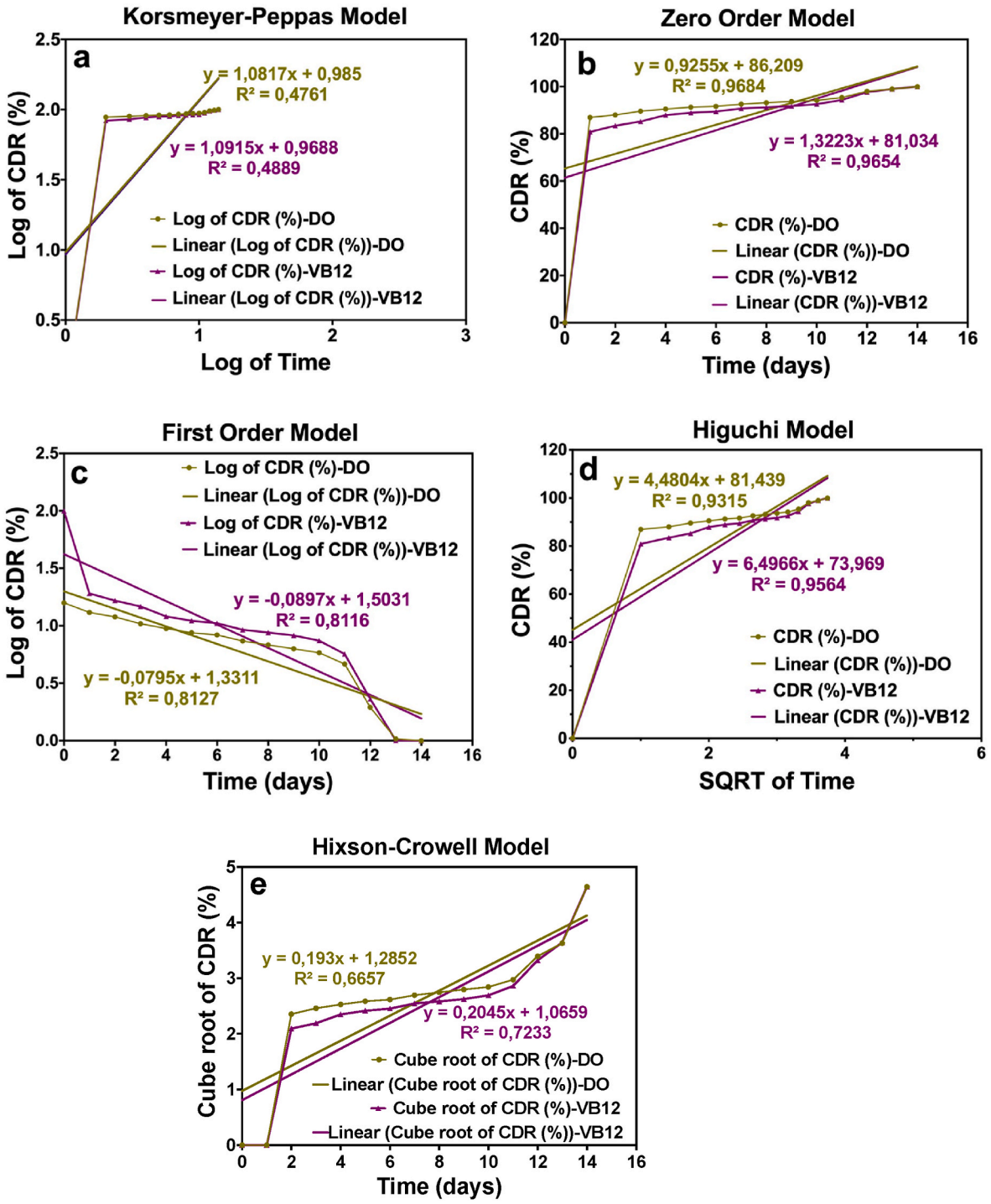

Fig. 7. The release kinetic models of DO and VB12 release profiles from DO/VB12-loaded NFs for 14 days: (a) Korsmeyer-Peppas, (b) zero order, (c) first order, (d) Higuchi, and (e) Hixon-Crowell models.

Table 3
Comparison of release mathematical models for DO/VB12-loaded NFs.

Sample		Korsmeyer-Peppas		Zero order		First order		Higuchi		Hixson-Crowell	
		R^2	n	R^2	K_0	R^2	K_1	R^2	K_h	R^2	K_{hc}
DO/VB12- loaded NFs	DO	0.476	1.081	0.968	0.926	0.812	−0.080	0.931	4.480	0.666	0.193
	VB12	0.489	1.091	0.965	1.322	0.811	−0.090	0.956	6.497	0.723	0.205

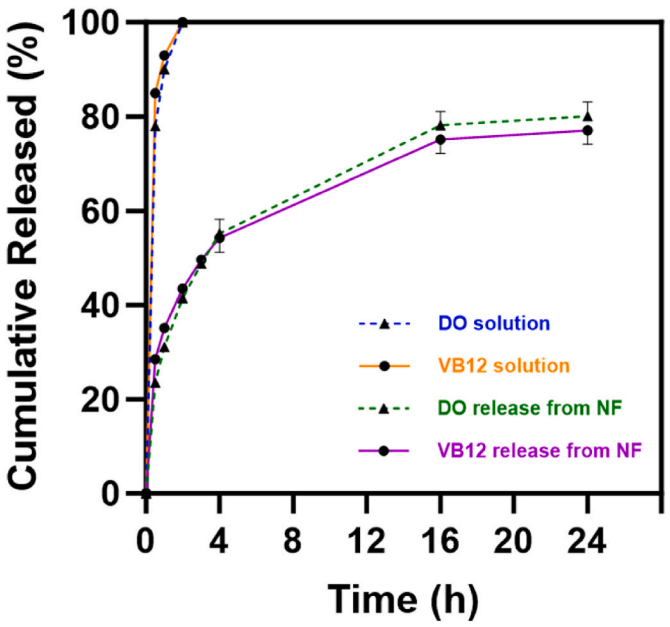

Fig. 8. The percentage of cumulative drug releases of DO and VB12 through a cellulose acetate membrane in Franz diffusion cell during 24 h.

with C–O–C asymmetric and symmetric stretching bands, and C–O–C symmetric stretching band at 1065 cm^{-1} all belong to PCL [39]. For pure PVP, the O–H stretching vibration band due to amide-iminol tautomerism was detected at 3403 cm^{-1} [27]. C–H asymmetric stretching band is assigned to CH_2 groups of the long aliphatic alkyl groups observed at 2950 cm^{-1} [40]. A characteristic amide C═O stretching vibration band at 1644 cm^{-1} shows the most intensive absorption. PVP spectra also have C–N stretching vibrations at 1460 and 1421 cm^{-1}, C–H bands at 1372 and 1317 cm^{-1}, the characteristic absorption band of C–N stretching at 1286 cm^{-1}, and weak CH_2 twist bands at 1228 and 1169 cm^{-1} [41]. From the spectra of DO, it was noticed that the basic functional groups of the compound are aromatic phenone and para-substituted aromatic hydrocarbon, and the same peaks were found in DO/VB12-loaded NFs as shown in Fig. 2. Aromatic C–H stretching bands at 2921 and 2857 cm^{-1}, the most intensive absorption band which was assigned to the stretching vibrations of C═O group at 1681 cm^{-1}, aromatic C═C stretching band at 1590 cm^{-1}, C–N stretching band with sharp absorption at 1313 cm^{-1}, C–O stretching band at 1037 cm^{-1}, aromatic C–H bending at 748 and 700 cm^{-1} were recorded for DO and DO/VB12-loaded NFs [42]. From the spectra of pure VB12, main bands were observed at the ranges of 2800–3500 cm^{-1} and 1000–1750 cm^{-1}, and characteristic absorption bands were observed at the 900–1800 cm^{-1} range. The O–H stretching band at 3274 cm^{-1}, C–H stretching band at 2923 cm^{-1}, C═O stretching band at 1642 cm^{-1}, C–H bending vibration at 1359 cm^{-1}, C–O stretching band at 1147 cm^{-1}, and PO_3^- symmetric stretching at 993 cm^{-1} were found [43,44].

3.3. X-ray diffraction analysis of fibers

The X-ray diffraction of PCL, PVP, DO, VB12, PF, and DO/VB12-loaded NFs was performed to investigate crystallization properties (Fig. 3). The crystallinity of a sample depends on the amount of sharp high-intensity peaks and when the high-intensity peaks have existed, crystallinity is high, however, the broader peak represents a high amorphous structure [45]. The XRD pattern of pure PCL showed strong characteristic peaks at Bragg angles $2\theta = 21.4°$ and 23.5° corresponding to its crystalline structure (Fig. 3c). As seen in Fig. 3d, due to the amorphous nature of PVP was detected at $2\theta = 11.6°$ and 21.7° with two broad diffraction humps [46]. In addition, sharp crystallinity peaks at 12.6°, 13.1°, 21.2°, 23.0°, and 24.0° were observed for pure DO (Fig. 3a). Also, DO crystalline structure might disrupt the amorphous nature of PVP. One of the diffraction humps revealing the amorphous character of pure VB12 was found at 21.3° (Fig. 3b) [47]. In the XRD profile of PF, sharp peaks of PCL were prominently seen (Fig. 3e). The broadness of the peaks increased slightly with the addition of DO and VB12. Also, the most intensive peaks of DO/B12-loaded fiber (21.6°, 24.0°) have shifted a slight degree concerning PF (21.4°, 23.6°).

3.4. Thermal properties

Thermograms for VB12 and DO compounds, PF, and DO/VB12-loaded NFs were acquired using DSC analysis (Fig. 4). The crystallization peak (Tc) at 29.9 °C and melting temperature (Tm) at 62.6 °C belonged to PCL that inside of the PF [48–50]. However, Tc and Tm values of PCL in DO/B12-loaded fiber were found to be 32.65 °C and 62.65 °C, respectively. As an amorphous polymer, PVP shows glass transition while melting [51]. However, any Tg peak related to PVP was not seen in PF. PVP-containing fibers do not show any peak or phase transition because of the dehydration [52]. Two endothermic peaks at 108.9 °C (Tg) and 228.2 °C (Tm) were observed for DO [53,54]. The thermogram of B12 starts water loss at 140.0 °C and shows a broad endotherm between 206.0 °C and 259.6 °C accompanied by melting and degradation [43,47].

3.5. Swelling and degradation assay

The release behaviours of DO and VB12 from the fiber depend on the swelling degree of fiber [55]. Fig. 5 was a representation of the swelling degree for PF and DO/VB12-loaded NFs. According to the result, PF is found to be higher than that of DO/VB12-loaded NFs. It is known that the addition of PVP to PCL increases the hydrophilicity of PCL, and because of this, the swelling rate of fiber is improved [56]. Fibers swelled during 12 h and after the 12th h, the swelling rate began to decrease. The highest swelling rate was observed for PF. The swelling rate was found to be decreased by drug loading. It can be said that after the 24th h, DO/VB12-loaded NFs may continue to swell for longer than PF.

3.6. Drug encapsulation efficiency and in vitro drug release assay

The amount of DO and VB12 released from DO/VB12-loaded NFs were investigated by UV spectroscopy using calibration curves, which are $y = 0.0286x - 0.0113$ and $y = 0.0094x - 0.0159$ for DO and VB12, respectively (Fig. 6a and b). DO and VB12 were rapidly released on the first day by ~84% and ~78%, respectively from DO/VB12-loaded NFs and there was continuous slow release for the following days (Fig. 6c). Interestingly, DO and VB12 showed similar release behaviour throughout the entire release period. On the 14th day, at the end of the study, the release both of DO and VB12 reached ~100% from DO/VB12-loaded NFs. The encapsulation efficiencies (EE) of DO and VB12 in DO/VB12-loaded NFs were 89.1% and 75.91%, respectively.

3.7. In vitro drug release kinetics

The profiling of *in vitro* drug release experiments is a critical instrument for giving notice of the drug release *in vivo* in advance. Fig. 7 indicates the drug release kinetic pattern of DO and VB12 from DO/VB12-loaded NFs and Korsmeyer-Peppas, first order, zero order, Higuchi, and Hixson-Crowell release patterns were utilized to explore release kinetics. Also, Table 3 involves kinetic constants and regression coefficients (R^2) belonging to DO/VB12-loaded NFs. The zero order equation is better in accord with the *in vitro* diffusion profiles for DO/VB12-loaded NFs (Fig. 7c).

The n value is used in the Korsmeyer-Peppas model to explain the drug release mechanism from a polymeric formulation. The diffusion

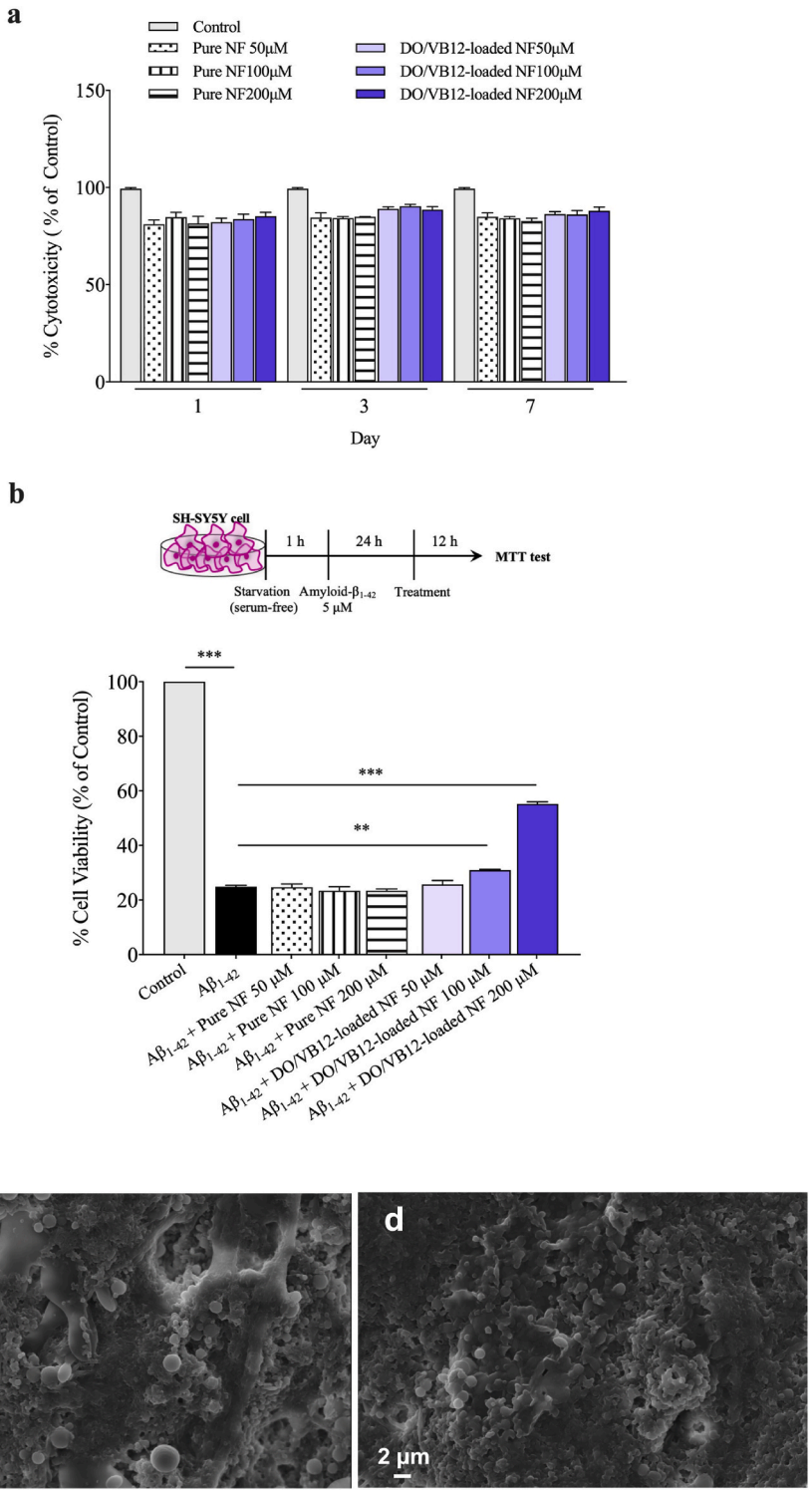

Fig. 9. Effect of DO/VB12-loaded NFs on the (a) cytotoxicity and (b) cell viability in the $A\beta_{1\text{-}42}$ fibrils. SEM images of cell clusters on (c) PF and (d) DO/VB12-loaded NFs.

component (n) value was higher than 1, which suggests the super case II transport of the drug from DO/VB12-loaded NFs [33].

3.8. Determination of membrane permeation

The quantity of DO and VB12 passed through the membrane of the Franz diffusion cell was measured using UV spectroscopy and calculated quantitatively over the calibration curves of DO and VB12 (Fig. 8). The membrane does not have an impact on drug diffusion from the liquid formulations of DO and VB12, which proves that an adequate membrane was chosen. The liquid formulations fastly passed through the membrane in 2 h. DO and VB12 successfully diffused through the membrane and the passed amounts of DO and VB12 were almost the same. While the cumulative release amount showed a rapid increase in the first 4 h, the increase slowed down in the following hours and reached 80% in 24 h. These results show that NFs provided a prolonged drug release and

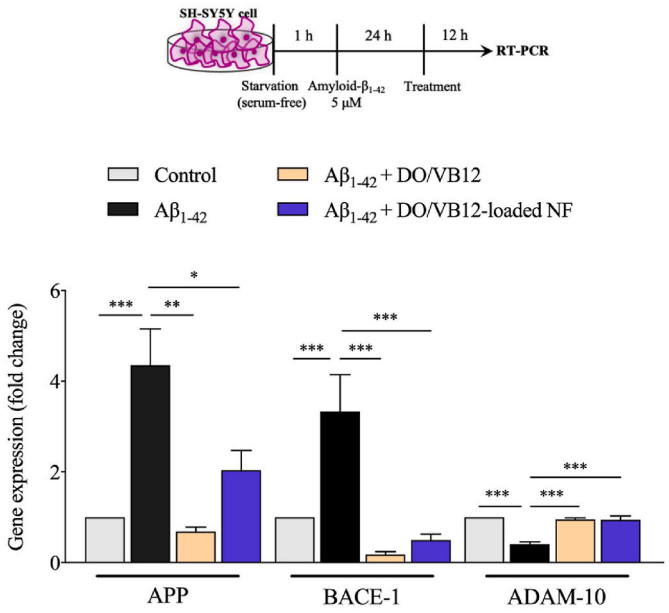

Fig. 10. Effects of DO/VB12-loaded NF treatment on the relative fold changes in APP, BACE-1, and ADAM-10 gene expressions.

DO/VB12-loaded NFs are proper for the transdermal application.

3.9. Cytotoxicity studies in SH-SY5Y cells

The cytotoxicity profile of DO/VB12-loaded NFs was studied in the SH-SY5Y cell line using an MTT assay. Three different concentrations (50, 100, and 200 μM) of each pure NFs and DO/VB12-loaded NFs were used for the MTT assay. From the results presented in Fig. 9a, the treatment of SH-SY5Y cells with 50, 100, and 200 μM DO/VB12-loaded NFs supported cell viability between 80 and 95%. The efficacy of DO/VB12-loaded NFs against amyloid-induced neurotoxicity was evaluated. Overall, DO/VB12-loaded NFs dose-dependently protected cells from $A\beta_{1\text{-}42}$-induced damage. As presented in Fig. 9b, cell viability was 24.87% by treatment with $A\beta_{1\text{-}42}$ treatment for 24 h. Pure NFs did not show a significant difference in cell viability compared to the $A\beta_{1\text{-}42}$-added group (50 μM pure NF-24.71%; 100 μM pure NFs −23.42%; 200 μM pure NFs −23.43%). There was no significant change in cell viability (25.6%) in the presence of DO/VB12-loaded NF at 50 μM concentration. The treatment with DO/VB12-loaded NFs showed only a small increase (30.9%) in cell survival at 100 μM. After treatments with 200 μM DO/VB12-loaded NFs, the observed cell viability rates were 55.24% in MTT. Comparison with pure NFs can reveal the effect of DO/VB12-loaded NFs as well as provide an interpretation of the impurities of both NFs. Based on this result, 200 μM DO/VB12-loaded NFs were able to protect SH-SY5Y cells at the most effective dose against amyloid-induced neurotoxicity. The confluent SH-SY5Y cells were observed by SEM and it was investigated that the cell clusters on PF (Fig. 9c) and DO/VB12-loaded NF (Fig. 9d) samples at 200 μM are properly proliferating. MTT test results of NFs are compatible with SEM images. The effect of DO/VB12-loaded NFs in cellular survival pathways allowed for further interpretation of these findings.

3.10. PCR results

Amyloid-β precursor protein (APP), the source of Aβ, can be proteolytically processed by ADAM-10 (α-secretase) and BACE-1 (β-secretase) in neurons. To identify the mechanisms underlying the regulation of $A\beta_{1\text{-}42}$ destruction by DO/VB12-loaded NFs, we examined the effects of DO/VB12-loaded NFs on APP, BACE-1, and ADAM-10 gene expression levels. As shown in Fig. 10, APP and BACE-1 gene expression increased while ADAM-10 expression remarkably decreased in $A\beta_{1\text{-}42}$-induced SH-SY5Y cells compared with the control. The results showed that DO/VB12-loaded NF (200 μM) significantly suppressed the expression of APP and BACE-1 ($p < 0.05$ and $p < 0.001$, respectively) of Aβ-activated cells (Fig. 10a–b). Furthermore, the DO/VB12-loaded NFs group showed a significant ($p < 0.001$) increase in the expression of ADAM-10. Also, the expression of BACE-1 and ADAM-10 indicates no significant difference when the DO/VB12-loaded NF group was compared with the DO/VB12-free drug-treated group. As is well known, the processing of APP by ADAM-10 in the non-amyloidogenic pathway produces ectodomain fragment (sAPPα), which has neuroprotective properties. Although a pharmacological approach has not yet emerged, ADAM-10 expression now offers a therapeutic option for AD. On the other hand, proteolytic cleavage of APP by BACE-1 in the amyloidogenic pathway produces neurotoxic Aβ. Achieving a decrease in BACE-1 expression is considered a target in drug treatments [57]. These data indicate that DO/VB12-loaded NFs can regulate Aβ-stimulated neurotoxicity by inhibiting amyloidogenic and non-amyloidogenic pathway formation in SH-SY5Y cells.

3.11. Confocal microscopy

The morphologies and nuclei of amyloid-induced SH-SY5Y cells treated with DO/VB12-loaded NFs were visualized under a confocal microscope (Fig. 11). Confocal images revealed cytoskeletal disintegration in amyloid-induced cells. On the other hand, nuclei with cytoskeleton were visualized in DO/VB12-loaded NFs.

4. Discussion

This study presents a combination therapy in a form suitable for drug release from the transdermal route and which can reduce Aβ deposition as a potential option for AD. In recent years, the development and *in vitro* evaluation of transdermal patches loaded with galantamine [58], rivastigmine [59], and donepezil [60] are valued as approaches to reduce patient complaints compared to the conventional dosage forms. In this study, our data demonstrated that DO/VB12-loaded NFs increased the viability of Amyloid-induced cells with prolonged drug release and showed protection against neurotoxicity by affecting the expressions of proteins in the amyloidogenic pathway. PCL/PVP fibers at six different concentrations were produced by pressurized gyration and compared to determine the optimized polymer ratio for DO/VB12-loaded NFs. Pressurized gyration (PG) is a fiber production method combining centrifugal spinning and solution-blowing techniques by using pressure, flow, and rotation. The resulting fiber diameter depends on the polymer solution properties and system parameters [61]. The working mechanism of the device is based on coming out of the polymer solution through the perforations of a rotating vessel and the fibers are obtained after the evaporation of the solvent. PG is superior to other fiber production methods in terms of producing bead-free fibers, providing a safe working area without using voltage, and offering mass production capability [62].

As per this work, solvent systems of six different ratios have been used to successfully produce PCL/PVP fibers by pressurized gyration method and the best ratio was chosen as the 15PF41 owing to superiority in morphology according to SEM images. On the other hand, we noticed that fiber diameter increased as the polymer content from 10% to 20%, as in another study in the literature. During fiber production, optimization is necessary to prevent polymer bead formation. Fabricating the smooth fiber morphologies needs acceptable polymer entanglement, and for a definite molecular weight, the entanglement density rises with the concentration of the polymer. In addition, increasing the polymer concentration will increase the viscosity, thus preventing the evaporation of the solvent, and this results in thicker fibers [63]. The decrease in the diameter of fibers with the addition of DO and B12 supported that 15PF41 was a suitable choice for drug loading.

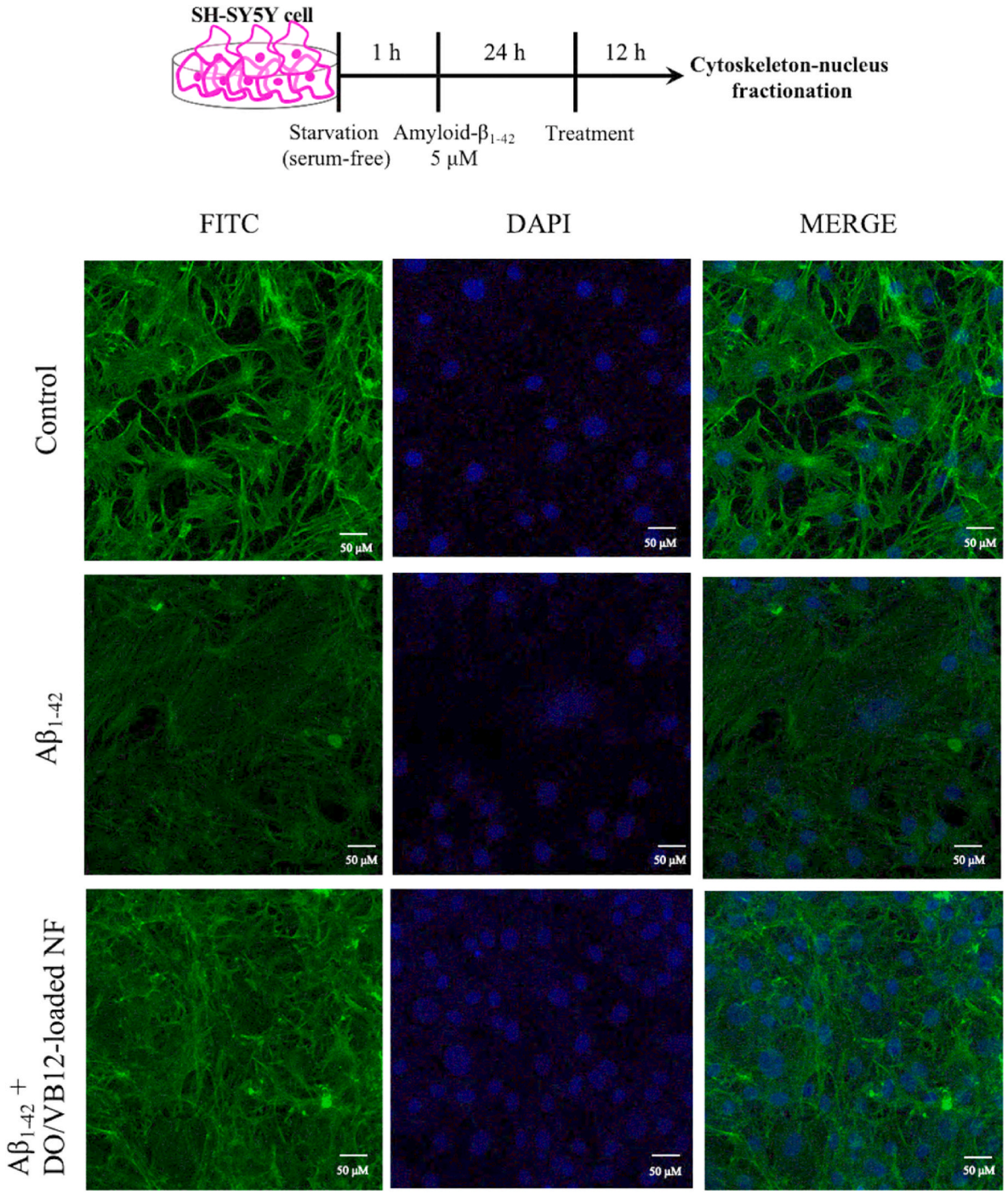

Fig. 11. Confocal microscopy images of DO/VB12-loaded NFs-treated SH-SY5Y cells. Cells were stained with DAPI to display nuclei (blue) and FITC to display cytoskeleton (green). Scale bar 50 μM. (For interpretation of the references to colour in this figure legend, the reader is referred to the Web version of this article.)

When the comparative FTIR results were investigated, the characteristic bands of all polymers and drugs were observed in the spectrums for PF and DO/VB12-loaded NFs, except for slight deviations in wavelengths. This might be due to the forming of new bonds of fibers produced by the pressurized gyration method. As a result, successful drug encapsulation has been accomplished. XRD analysis revealed that DO and PCL diffraction patterns have sharp crystalline peaks while B12 and PVP have shown an amorphous profile. The disappearance of sharp characteristic DO (a hydrochloride salt) peaks in DO/VB12-loaded NFs can be linked to the deterioration of the crystal structure of the salts when complexing with polymers [64]. Achievement result was obtained by reducing the crystallinity of DO by producing DO/B12-loaded fiber. Although DO/VB12-loaded NFs showed a similar XRD profile to PF, it is possible to say that DO and VB12 successfully loaded in PF. Taken together, these results suggest that VB12 and PVP have an amorphous structure, it is normal for only PCL peaks to appear in DO/VB12-loaded NFs, similar to those in PF [65].

According to DSC results, endothermic peaks shifted with drug loading due to physical or chemical interactions between drugs and polymers [66]. In addition, according to the XRD results, PCL is a crystalline polymer, which is also confirmed by a sharp endothermic peak in the DSC results of PF and DO/VB12-loaded NFs. In the literature, the endothermic peak of pure PCL fibers was at 60 °C [67]. The findings of this study suggest that the endothermic peak of PF at 62.65 °C and the

peak of DO/B12-loaded NFs at 64.95 °C are due to the PVP effect. A possible explanation for these results may be that it has been shown in the literature that the Tg peak of pure PCL fibers occurs at 100 °C, and in our study, this resulted in the fusion of the Tm peak of PCL and the Tg peak of PVP. The findings of this study suggest that the shift in the endothermic peak depends on Tm and Tg fusion [67].

Although the swelling behaviour of PF and DO/VB12-loaded NFs showed a similar profile, the water-holding capacity of PFs was found to be higher than that of DO/VB12-loaded NFs. The data reported here appear to support the assumption that drug loading reduces the water-holding capacity of the NFs. On the other hand, in our study, it is also seen that the release and swelling behaviour profiles are similar. DO and VB12 release rate from DO/VB12-loaded NFs depends on the diffusion across the skin and the decreased swelling rate by drug loading can be related to the low skin permeability of hydrophilic DO. This result appears to support the hypothesis that drug-release behaviour depends on the degree of swelling [9,65].

During *in vitro* drug release study, DO and VB12 showed similar release behaviour with the burst release on the first day followed by a continuous slow release for 14 days. As it is well known, hydrophilic drugs such as DO and VB12 show a rapid release due to their higher solubility in an aqueous medium. However, the hydrophobic nature of PCL supported the sustained release profile of the drugs [22]. Although burst release followed by a sustained release of V12 and DO was achieved with PCL-based NF systems in previous studies, the DO and VB12 releases from NFs reaching 100% as in our results cannot be obtained in other NF formulations [22,68]. Another significant aspect of the sustained release of drugs from DO/VB12-loaded NFs is to keep the concentration of the drug in the site of action constant to propose a solution to current bioavailability problems. This result proved that the drug release behaviour can be managed by polymer choice. *In vitro* drug release kinetics presented that the zero order model has better agreement with DO/VB12-loaded NFs. The value of n was higher than 1 indicating drugs were released from nanofibers through the super case II transport [66]. According to the Franz diffusion cell results, DO and VB12 successfully diffused through the membrane with a pore size of 0.45 μm and it is thought that the drugs in DO/VB12-loaded NFs can penetrate the human skin with an average pore size of 40–80 μm [69]. The results show that NFs provided a prolonged drug release from a cellulose acetate membrane, which mimics the human skin, and DO/VB12-loaded NFs are proper for the transdermal application.

The fact that DO/VB12-loaded NFs did not show any differential effect on viability in the absence of Aβ indicates that the pure and drug-loaded fibers do not have a toxic effect. This result made it possible to perform other tests safely, as there was no effect on the viability caused by the NFs. We used the MTT assay to examine whether a reduction in the content of fibril actions of NFs was involved in the neuroprotective effect against Aβ-mediated toxicity in cells. Aβ-induced neuronal cell death is considered to be a critical event in the pathogenesis of AD. According to MTT assay results, DO/VB12-loaded NFs showed a potential dose-dependent cytoprotective activity against $A\beta_{1\text{-}42}$-induced toxicity in cells. In recent years, studies have made remarkable evaluations that DO improves cognitive functions *in vivo* AD models by preventing Aβ accumulation [70]. These studies have shown that DO can inhibit Aβ accumulation by direct mitochondrial protection against $A\beta_{1\text{-}42}$ damage, independent of its specific effect on AChE. In addition, experimental data showing that VB12 delays Aβ fibrillation, reduces the content of fibrils, and disrupts mature fibrils *in vitro* indicates that it may be a promising drug candidate to prevent and treat AD [14]. As an extension of previous works, the current study confirmed that NFs protect cells against Aβ-associated cell death by the dual-drug release of DO and VB12 from drug-loaded NFs *in vitro* model.

It was concluded that DO/VB12-loaded NFs exhibited dose-dependent neuronal protection in amyloid-induced neurotoxicity. We evaluated the possible potential mechanism of this action of the drug-loaded NFs by RT-PCR analysis. The proteolytic cleavage of APP by BACE-1(β-secretase) and ADAM-10 (α-secretase) in the amyloidogenic/non-amyloidogenic pathway is the limiting step in cells for the formation of the Aβ peptide which is the hallmark of AD [70]. APP is hydrolyzed by BACE-1 to form $A\beta_{1\text{-}40}$ and $A\beta_{1\text{-}42}$ fragments. $A\beta_{1\text{-}42}$ is responsible for amyloid plaque formation and AD-like lesions in the brain due to its neurotoxic effect. The expression level of APP, BACE-1, and ADAM-10 genes are associated with the pathogenesis of AD [71]. Clinical and preclinical studies have provided links that excessive accumulation of amyloid peptides in neurons is due to proteolytic cleavage of APP via the secretase enzymes, which has been attributed to a significant increase in neuroinflammation by impaired cognitive abilities, and oxidative stress [72]. Experimental studies indicate that the determination of APP, BACE-1, and ADAM-10 expression levels in SH-SY5Y cells after incubation with Amyloid reflects neuronal toxicity. According to our results, DO/VB12-loaded NFs treatment can decrease APP and BACE-1 and increase ADAM-10 expression levels in the cell. Fuso et al. [15] showed that VB12 deficiency causes increased BACE-1 expression, which is associated with increased Aβ levels. This is the first proof, which declares that certain DO/VB12-loaded NFs would have a positive impact on the inhibition of amyloid peptide formation.

5. Conclusion

In this study, an original long-acting biocompatible DO/VB12-loaded NFs was prepared by pressured gyration technique. Our study is the first to produce DO and VB12 in a single formulation in an extended-release form and present its efficacy on gene expression levels in an *in vitro* AD model. The results showed that DO/VB12-loaded NFs had favourable bead-free surface morphology and stable structure which was confirmed by thermal analysis, FTIR analysis, and swelling-degradation analysis. The drug release curve points to the conclusion that NFs can be seen as compatible with transdermal drug carriers since they show a rapid first-day release and sustained long-release profile. From the outputs of the present work, it can be concluded that the novel DO/VB12-loaded NFs was not toxic to cells and dose-dependently protected SH-SY5Y cells from $A\beta_{1\text{-}42}$-induced toxicity. Moreover, according to the results of RT-PCR arrays, NFs can inhibit amyloid formation by reducing gene expressions of APP and secretases. This study provides a new perspective on DO/VB12-loaded NFs as a drug delivery system that increases the applicability of potential drugs and improves patient compliance and product stability in the treatment of AD. All of the discussed data indicate that there is a need to elucidate the molecular mechanism of this new transdermal drug delivery system by detailing its effect on drug pharmacokinetics, blood-brain barrier permeability, and biological processes related to AD.

Credit author statement

Busra Ertas: Investigation, Data curation, Visualization, Writing – original draft. Irem Nur Onay: Methodology, Validation, Data curation. Ayse Mine Yılmaz-Goler: Methodology, Validation, Data curation. Betul Karademir-Yilmaz: Investigation, Resources, Formal analysis. Muhammet Emin Cam: Resources, Supervision, Supervising, Writing – review & editing.

Declaration of competing interest

The authors declare that they have no known competing financial interests or personal relationships that could have appeared to influence the work reported in this paper.

Data availability

The authors do not have permission to share data.

Acknowledgment

This study was supported by a TUBITAK 2209-A Research Projects Program Grant (2209-A, 2020/2, No: 1919B012002427, Scientific and Technological Research Council of Turkey-TUBITAK).

References

[1] A.M. Abo-Youssef, W.A. Khallaf, M.M. Khattab, B.A.S. Messiha, The anti-Alzheimer effect of telmisartan in a hyperglycemic ovariectomized rat model; role of central angiotensin and estrogen receptors, Food Chem. Toxicol. 142 (2020), 111441.
[2] A.S.D International, World Alzheimer Report, 2015 Available online: https://www.alz.co.uk/research/statistics. (Accessed 7 August 2022).
[3] S.G. Jeon, M.Y. Cha, J.I. Kim, T.W. Hwang, K.A. Kim, T.H. Kim, K.C. Song, J.J. Kim, M. Moon, Vitamin D-binding protein-loaded PLGA nanoparticles suppress Alzheimer's disease-related pathology in 5XFAD mice, Nanomedicine 17 (2019) 297–307.
[4] F. Topal, B. Ertas, E. Guler, F. Gurbuz, G.S. Ozcan, O. Aydemir, V.G. Bocekci, G. Duruksu, C. Sahin Cam, Y. Yazir, O. Gunduz, M.E. Cam, A novel multi-target strategy for Alzheimer's disease treatment via sublingual route: donepezil/memantine/curcumin-loaded nanofibers, Biomater. Adv. 138 (2022), 212870.
[5] N. Bassil, G.T. Grossberg, Novel regimens and delivery systems in the pharmacological treatment of Alzheimer's disease, CNS Drugs 23 (4) (2009) 293–307.
[6] M.E. Hasselmo, The role of acetylcholine in learning and memory, Curr. Opin. Neurobiol. 16 (6) (2006) 710–715.
[7] S. Cesur, M.E. Cam, F.S. Sayin, O. Gunduz, Electrically controlled drug release of donepezil and BiFeO3 magnetic nanoparticle-loaded PVA microbubbles/nanoparticles for the treatment of Alzheimer's disease, J. Drug Deliv. Sci. Technol. 67 (2022), 102977.
[8] H.G. Kim, M. Moon, J.G. Choi, G. Park, A.J. Kim, J. Hur, K.T. Lee, M.S. Oh, Donepezil inhibits the amyloid-beta oligomer-induced microglial activation in vitro and in vivo, Neurotoxicology 40 (2014) 23–32.
[9] P. Sozio, L.S. Cerasa, L. Marinelli, A. Di Stefano, Transdermal donepezil on the treatment of Alzheimer's disease, Neuropsychiatric Dis. Treat. 8 (2012) 361–368.
[10] J. Mehrdad, E. Leila, N. Emsehgol, The effect of vitamin B12 on synaptic plasticity of hippocampus in Alzheimer's disease model rats, Int. J. Neurosci. (2021) 1–6.
[11] M. Wang, T. Xu, Methyl B12 protects PC12 cells against cytotoxicity induced by Aβ (25-35), J. Cell. Biochem. 120 (2019) 11921–11930.
[12] F. Ma, X. Zhou, Q. Li, J. Zhao, A. Song, P. An, Y. Du, W. Xu, G. Huang, Effects of folic acid and vitamin B12, alone and in combination on cognitive function and inflammatory factors in the elderly with mild cognitive impairment: a single-blind experimental design, Curr. Alzheimer Res. 16 (7) (2019) 622–632.
[13] A.B. Lam, K. Kervin, J.E. Tanis, Vitamin B(12) impacts amyloid beta-induced proteotoxicity by regulating the methionine/S-adenosylmethionine cycle, Cell Rep. 36 (13) (2021), 109753.
[14] S. Andrade, J.A. Loureiro, M.C. Pereira, Vitamin B12 inhibits Aβ fibrillation and disaggregates preformed fibrils in the presence of synthetic neuronal membranes, ACS Chem. Neurosci. 12 (13) (2021) 2491–2502.
[15] A. Fuso, L. Seminara, R.A. Cavallaro, F. D'Anselmi, S. Scarpa, S-adenosylmethionine/homocysteine cycle alterations modify DNA methylation status with consequent deregulation of PS1 and BACE and beta-amyloid production, Mol. Cell. Neurosci. 28 (1) (2005) 195–204.
[16] S. Andrade, M.J. Ramalho, J.A. Loureiro, M.C. Pereira, Transferrin-functionalized liposomes loaded with vitamin VB12 for Alzheimer's disease therapy, Int. J. Pharm. (2022), 122167.
[17] K.S. V G, S.G.S.S. Sureshkumar, D.S. Preethikrishnan, B.D. S.A, V.P. Riya, Therapeutic impact of rHuEPO on abnormal platelet APP, BACE 1, presenilin 1, ADAM 10 and Aβ expressions in chronic kidney disease patients with cognitive dysfunction like Alzheimer's disease: a pilot study, Biomed. Pharmacother. 104 (2018) 211–222.
[18] S. Bashyal, C.Y. Shin, S.M. Hyun, S.W. Jang, S. Lee, Preparation, characterization, and in vivo pharmacokinetic evaluation of polyvinyl alcohol and polyvinyl pyrrolidone blended hydrogels for transdermal delivery of donepezil HCl, Pharmaceutics 12 (3) (2020).
[19] G. Small, B. Dubois, A review of compliance to treatment in Alzheimer's disease: potential benefits of a transdermal patch, Curr. Med. Res. Opin. 23 (11) (2007) 2705–2713.
[20] E.L. Doets, P.H. in 't Veld, A. Szczecińska, R.A.M. Dhonukshe-Rutten, A.E.J. M. Cavelaars, P. van 't Veer, A. Brzozowska, L.C.P.G.M. de Groot, Systematic review on daily vitamin B12 losses and bioavailability for deriving recommendations on vitamin B12 intake with the factorial approach, Ann. Nutr. Metab. 62 (4) (2013) 311–322.
[21] S. Oh, G. Cave, C. Lu, Vitamin B(12) (cobalamin) and micronutrient fortification in food crops using nanoparticle technology, Front. Plant Sci. 12 (2021), 668819.
[22] K. Madhaiyan, R. Sridhar, S. Sundarrajan, J.R. Venugopal, S. Ramakrishna, Vitamin B12 loaded polycaprolactone nanofibers: a novel transdermal route for the water soluble energy supplement delivery, Int. J. Pharm. 444 (1–2) (2013) 70–76.
[23] F. Sabbagh, B.S. Kim, Recent advances in polymeric transdermal drug delivery systems, JCR 341 (2022) 132–146.
[24] M.E. Cam, S. Yildiz, H. Alenezi, S. Cesur, G.S. Ozcan, G. Erdemir, U. Edirisinghe, D. Akakin, D.S. Kuruca, L. Kabasakal, O. Gunduz, M. Edirisinghe, Evaluation of burst release and sustained release of pioglitazone-loaded fibrous mats on diabetic wound healing: an in vitro and in vivo comparison study, J. R. Soc. Interface 17 (162) (2020), 20190712.
[25] H. Alenezi, M.E. Cam, M. Edirisinghe, Experimental and theoretical investigation of the fluid behavior during polymeric fiber formation with and without pressure, Appl. Phys. Rev. 6 (2019), 041401.
[26] G.M. Kim, K.H. Le, S.M. Giannitelli, Y.J. Lee, A. Rainer, M. Trombetta, Electrospinning of PCL/PVP blends for tissue engineering scaffolds, J. Mater. Sci. Mater. Med. 24 (6) (2013) 1425–1442.
[27] M.E. Cam, B. Ertas, H. Alenezi, A.N. Hazar-Yavuz, S. Cesur, G.S. Ozcan, C. Ekentok, E. Guler, C. Katsakouli, Z. Demirbas, D. Akakin, M.S. Eroglu, L. Kabasakal, O. Gunduz, M. Edirisinghe, Accelerated diabetic wound healing by topical application of combination oral antidiabetic agents-loaded nanofibrous scaffolds: an in vitro and in vivo evaluation study, Mater Sci. Eng. C Mater Biol. Appl. 119 (2021), 111586.
[28] N.E. Zander, Formation of melt and solution spun polycaprolactone fibers by centrifugal spinning, J. Appl. Polym. Sci. 132 (2) (2014).
[29] U.E. Illangakoon, H. Gill, G.C. Shearman, M. Parhizkar, S. Mahalingam, N. P. Chatterton, G.R. Williams, Fast dissolving paracetamol/caffeine nanofibers prepared by electrospinning, Int. J. Pharm. 477 (1) (2014) 369–379.
[30] Z. Yang, X. Li, J. Si, Z. Cui, K. Peng, Morphological, mechanical and thermal properties of poly(lactic acid) (PLA)/Cellulose nanofibrils (CNF) composites nanofiber for tissue engineering, J. Wuhan Univ. Technol.-Materials Sci. Ed. 34 (1) (2019) 207–215.
[31] Z.K. Nagy, K. Nyul, I. Wagner, K. Molnar, G. Marosi, Electrospun water soluble polymer mat for ultrafast release of Donepezil HCl, Express Polym. Lett. 4 (12) (2010) 763–772.
[32] E. Ilhan, S. Cesur, E. Guler, F. Topal, D. Albayrak, M.M. Guncu, M.E. Cam, T. Taskin, H.T. Sasmazel, B. Aksu, F.N. Oktar, O. Gunduz, Development of Satureja cuneifolia-loaded sodium alginate/polyethylene glycol scaffolds produced by 3D-printing technology as a diabetic wound dressing material, Int. J. Biol. Macromol. 161 (2020) 1040–1054.
[33] S. Dash, P.N. Murthy, L. Nath, P. Chowdhury, Kinetic modeling on drug release from controlled drug delivery systems, Acta Pol. Pharm. 67 (3) (2010) 217–223.
[34] L. Bartosova, J. Bajgar, Transdermal drug delivery in vitro using diffusion cells, Curr. Med. Chem. 19 (27) (2012) 4671–4677.
[35] M.E. Cam, A.N. Hazar-Yavuz, S. Cesur, O. Ozkan, H. Alenezi, H. Turkoglu Sasmazel, M. Sayip Eroglu, F. Brako, J. Ahmed, L. Kabasakal, G. Ren, O. Gunduz, M. Edirisinghe, A novel treatment strategy for preterm birth: intra-vaginal progesterone-loaded fibrous patches, Int. J. Pharm. 588 (2020), 119782.
[36] F. Gao, J. Zhao, P. Liu, D. Ji, L. Zhang, M. Zhang, Y. Li, Y. Xiao, Preparation and in vitro evaluation of multi-target-directed selenium-chondroitin sulfate nanoparticles in protecting against the Alzheimer's disease, Int. J. Biol. Macromol. 142 (2020) 265–276.
[37] P. Alam, M.K. Siddiqi, S.K. Chaturvedi, M. Zaman, R.H. Khan, Vitamin B12 offers neuronal cell protection by inhibiting Aβ-42 amyloid fibrillation, Int. J. Biol. Macromol. 99 (2017) 477–482.
[38] Y. Wang, Y. Liu, Y. Qian, L. Lv, X. Li, Y. Liu, Characteristics of MgO/PCL/PVP antibacterial nanofiber membranes produced by electrospinning technology, Surface. Interfac. 28 (2022), 101661.
[39] X. Wang, H. Zhao, L.-S. Turng, Q. Li, Crystalline morphology of electrospun poly (ε-caprolactone) (PCL) nanofibers, Ind. Eng. Chem. Res. 52 (13) (2013) 4939–4949.
[40] D.S.A. Fakhrali, H. Salehi, M. Ghane, Electrospun PGS/PCL nanofibers: from straight to sponge and spring-like morphology, Polym. Adv. Technol. 31 (12) (2020) 3134–3149.
[41] B.T. Raimi-Abraham, S. Mahalingam, M. Edirisinghe, D.Q. Craig, Generation of poly(N-vinylpyrrolidone) nanofibres using pressurised gyration, Mater Sci. Eng. C Mater Biol. Appl. 39 (2014) 168–176.
[42] A. Gencturk, A.S. Sarac, Determination of donepezil HCl release from electrospun fiber by electrochemical impedance spectroscopy, Int. J. Electrochem. Sci. 11 (2016) 111–125.
[43] M. Gharagozlou, S. Naghibi, Preparation of vitamin B12–TiO2 nanohybrid studied by TEM, FTIR and optical analysis techniques, Mater. Sci. Semicond. 35 (2015) 166–173.
[44] L. Jin, P. Lu, H. You, Q. Chen, J. Dong, Vitamin B12 diffusion and binding in crosslinked poly(acrylic acid)s and poly(acrylic acid-co-N-vinyl pyrrolidinone)s, Int. J. Pharm. 371 (1–2) (2009) 82–88.
[45] S.R. Bajaj, R.S. Singhal, Enhancement of stability of vitamin B12 by co-crystallization: a convenient and palatable form of fortification, J. Food Eng. 291 (2021), 110231.
[46] M.A.Q. Bhuiyan, S. Rahman, M.S. Rahaman, M. Shajahan, N.C. Dafader, Improvement of swelling behaviour of poly (vinyl pyrrolidone) and acrylic acid blend hydrogel prepared by the application of gamma radiation, Org. Chem. 4 (2) (2015), 1000138.
[47] A. Baskakova, S. Awwad, J.Q. Jiménez, H. Gill, O. Novikov, P.T. Khaw, S. Brocchini, E. Zhilyakova, G.R. Williams, Electrospun formulations of acyclovir, ciprofloxacin and cyanocobalamin for ocular drug delivery, Int. J. Pharm. 502 (1–2) (2016) 208–218.
[48] A. Huang, Y.-C. Jiang, B. Napiwocki, H.-Y. Mi, X. Peng, L.-S. Turng, Fabrication of poly(ε-caprolactone) tissue engineering scaffolds with fibrillated and interconnected pores utilizing microcellular injection molding and polymer leaching, RSC Adv. 7 (2017) 43432–43444.
[49] S. Sánchez-González, N. Diban, A. Urtiaga, Hydrolytic degradation and mechanical stability of poly(ε-caprolactone)/reduced graphene oxide membranes as scaffolds for in vitro neural tissue regeneration, Membranes 8 (1) (2018).

[50] C.R. Reshmi, P. Sagitha, Sheeja, A. Sujith, Poly ϵ-caprolactone/nanostarch composite nanofibrous wound dressing with antibacterial property and pH stimulus drug release, Cellulose 29 (1) (2022) 427–443.
[51] W.S. Khan, R. Asmatulu, M.M. Eltabey, Electrical and thermal characterization of electrospun PVP nanocomposite fibers, J. Nanomater. 2013 (2013), 160931.
[52] X.-F.Z. Deng-Guang Yu, Xia-Xia Shen, Chris Brandford-White, Li-Min Zhu, Ultrafine ibuprofen-loaded polyvinylpyrrolidone fiber mats using electrospinning, Polym. Int. 58 (9) (2009) 1010–1013.
[53] M.C. Chuong, C.J. Kelley, Y. Muhammad, T.D. Caputo, J.M. Gomes, D. Oliveira, A. C. Peixoto, B.S. Pereira, W. Rizg, C. Vazquez, T.M. Zacaron, S. Nguyen, D. A. Williams, Investigating effect of water of hydration on active pharmaceutical ingredients in a water-sensitive dosage form, J. Appl. Sci. Technol. 9 (1) (2018) 7.
[54] A. Gencturk, Donepezil Hcl Loaded Electrospun Fibers for Transdermal Drug Delivery Systems, Department of Polymer Science and Technology, Istanbul Technical University, 2019.
[55] B. Singh, T. Garg, A.K. Goyal, G. Rath, Development, optimization, and characterization of polymeric electrospun nanofiber: a new attempt in sublingual delivery of nicorandil for the management of angina pectoris, Artif. Cells, Nanomed. Biotechnol. 44 (6) (2016) 1498–1507.
[56] R. PranavKumar Shadamarshan, H. Balaji, H.S. Rao, K. Balagangadharan, S. Viji Chandran, N. Selvamurugan, Fabrication of PCL/PVP electrospun fibers loaded with trans-anethole for bone regeneration in vitro, Colloids Surf., B 171 (2018) 698–706.
[57] X.Z. Yuan, S. Sun, C.C. Tan, J.T. Yu, L. Tan, The role of ADAM10 in Alzheimer's disease, J. Alzheimers Dis. 58 (2) (2017) 303–322.
[58] D. Ameen, B. Michniak-Kohn, Development and in vitro evaluation of pressure sensitive adhesive patch for the transdermal delivery of galantamine: effect of penetration enhancers and crystallization inhibition, Eur. J. Pharm. Biopharm. 139 (2019) 262–271.
[59] Y. Cai, Q. Tian, C. Liu, L. Fang, Development of long-acting rivastigmine drug-in-adhesive patch utilizing ion-pair strategy and characterization of controlled release mechanism, Eur. J. Pharmaceut. Sci. 161 (2021), 105774.
[60] L. Dinh, S. Lee, S.M. Abuzar, H. Park, S.J. Hwang, Formulation, preparation, characterization, and evaluation of dicarboxylic ionic liquid donepezil transdermal patches, Pharmaceutics 14 (1) (2022).
[61] S. Mahalingam, M. Edirisinghe, Forming of polymer nanofibers by a pressurised gyration process, Macromol. Rapid Commun. 34 (14) (2013) 1134–1139.
[62] P.L. Heseltine, J. Ahmed, M. Edirisinghe, Developments in pressurized gyration for the mass production of polymeric fibers, Macromol. Mater. Eng. 303 (9) (2018), 1800218.
[63] S. Mahalingam, S. Homer-Vanniasinkam, M. Edirisinghe, Novel pressurised gyration device for making core-sheath polymer fibres, Mater. Des. 178 (2019), 107846.
[64] V. Naranappa, S. Subramanian, N. Hellar, S. Chinnappanadar, Proton Conducting Polymer Electrolyte Based on Poly (N-Vinyl Pyrrolidone) Doped with Ammonium Iodide, 2015.
[65] R. Ravikumar, M. Ganesh, V. Senthil, Y.V. Ramesh, S.L. Jakki, E.Y. Choi, Tetrahydro curcumin loaded PCL-PEG electrospun transdermal nanofiber patch: preparation, characterization, and in vitro diffusion evaluations, J. Drug Deliv. Sci. Technol. 44 (2018) 342–348.
[66] S. Erzengin, E. Guler, E. Eser, E.B. Polat, O. Gunduz, M.E. Cam, In vitro and in vivo evaluation of 3D printed sodium alginate/polyethylene glycol scaffolds for sublingual delivery of insulin: preparation, characterization, and pharmacokinetics, Int. J. Biol. Macromol. 204 (2022) 429–440.
[67] H. Majd, A. Harker, M. Edirisinghe, M. Parhizkar, Optimised release of tetracycline hydrochloride from core-sheath fibres produced by pressurised gyration, J. Drug Deliv. Sci. Technol. 72 (2022), 103359.
[68] S. Aydin, I. Kabaoglu, E. Guler, F. Topal, A.N. Hazar-Yavuz, C. Ekentok, E. Tatar, F. Gurbuz, O. Gunduz, M.E. Cam, A comparison study of fiber diameter's effect on characteristic features of donepezil/curcumin-loaded polycaprolactone/polylactic acid nanofibers, Macromol. Mater. Eng. (2022), 2100855.
[69] U. Cizauskaite, J. Bernatoniene, Innovative natural ingredients-based multiple emulsions: the effect on human skin moisture, sebum content, pore size and pigmentation, Molecules 23 (6) (2018).
[70] S. Zameer, M. Kaundal, D. Vohora, J. Ali, A. Kalam Najmi, M. Akhtar, Ameliorative effect of alendronate against intracerebroventricular streptozotocin induced alteration in neurobehavioral, neuroinflammation and biochemical parameters with emphasis on Aβ and BACE-1, Neurotoxicology 70 (2019) 122–134.
[71] H. Turkez, I. Cacciatore, L. Marinelli, E. Fornasari, M.E. Aslan, K. Cadirci, C. Y. Kahraman, O. Caglar, A. Tatar, G. Di Biase, A. Hacimuftuoglu, A. Di Stefano, A. Mardinoglu, Glycyl-L-prolyl-L-glutamate pseudotripeptides for treatment of Alzheimer's disease, Biomolecules 11 (1) (2021).
[72] S. Wu, H. Liu, H. Zhao, X. Wang, J. Chen, D. Xia, C. Xiao, J. Cheng, Z. Zhao, Y. He, Environmental lead exposure aggravates the progression of Alzheimer's disease in mice by targeting on blood brain barrier, Toxicol. Lett. 319 (2020) 138–147.